PHYSICAL REVIEW B **94**, 121105(R) (2016)

Hybrid Weyl semimetal

Fei-Ye Li,[1] Xi Luo,[1] Xi Dai,[2] Yue Yu,[3,5] Fan Zhang,[4] and Gang Chen[3,5,*]

[1]*CAS Key Laboratory of Theoretical Physics, Institute of Theoretical Physics, Chinese Academy of Sciences, Beijing 100190, People's Republic of China*

[2]*Beijing National Laboratory for Condensed Matter Physics, and Institute of Physics, Chinese Academy of Sciences, Collaborative Innovation Center of Quantum Matter, Beijing 100190, People's Republic of China*

[3]*State Key Laboratory of Surface Physics, Center for Field Theory and Particle Physics, Department of Physics, Fudan University, Shanghai 200433, People's Republic of China*

[4]*Department of Physics, University of Texas at Dallas, Richardson, Texas 75080, USA*

[5]*Collaborative Innovation Center of Advanced Microstructures, Nanjing 210093, People's Republic of China*

(Received 1 August 2016; published 6 September 2016)

We construct a tight-binding model realizing one pair of Weyl nodes and three distinct Weyl semimetals. In the type-I (type-II) Weyl semimetal, both nodes belong to type-I (type-II) Weyl nodes. In addition, there exists a third type, previously undiscovered and dubbed "hybrid Weyl semimetal", in which one Weyl node is of type I while the other is of type II. For the hybrid Weyl semimetal, we further demonstrate the bulk Fermi surfaces and the topologically protected surface states, analyze the unique Landau-level structure and quantum oscillation, and discuss the conditions for possible material realization.

DOI: 10.1103/PhysRevB.94.121105

Introduction. Since the theoretical and experimental discovery of topological insulator [1,2], the study of topological states of matter has become one of the major topics in condensed-matter physics. Apart from the triumphs of systems with full energy gaps, the concept and discovery of Weyl semimetals (WSMs) have stimulated intensive activities in understanding the band topology for gapless systems [3–18]. A WSM, in the original setting, has linear conic band crossings at the Fermi energy [5]. These band crossing points, i.e., the "Weyl nodes", behave like sources and sinks of the Berry curvature in the momentum space and are topologically protected. Based on the bulk-boundary correspondence, the surface state of a WSM takes the form of Fermi arc that connects a pair of Weyl points with opposite chiralities [5].

A type of structured Weyl node, dubbed type II, was recently discovered in WTe_2 [14] and a spin-orbit-coupled superfluid [15]. In the original WSM, referred as type I, the Fermi surface is composed of discrete Weyl points with emergent Lorentz invariance. In type-II WSMs, the conic spectrum is tilted near the nodes, and the emergent Lorentz invariance is broken. These Lorentz-invariance-violating type-II Weyl nodes appear at the contact points of the electron and hole pockets in type-II WSMs. In all the previous works on type-I or type-II WSMs, the two Weyl nodes in a pair with opposite chiralities are of the same type [14,19]. One may wonder whether it is possible to have a WSM such that one Weyl node belongs to type I whereas its chiral partner belongs to type II (see Fig. 1). In this Rapid Communication, we analyze the band topology of a concrete lattice model and demonstrate that the proposed WSM phase with mixed types of Weyl nodes can be realized in the concrete model. We dub this special type of WSM "hybrid WSM". Remarkably, it is possible to have a *single isolated Weyl fermion* in the excitation spectrum of this hybrid WSM rather than several pairs of Weyl fermions in the conventional case. We explicitly show that the band structure contains two Weyl nodes, whose types can be tuned separately and independently. Therefore, our model provides a simple platform to manipulate the energy-momentum positions, the types of Weyl nodes, and the transitions among different types of WSMs. We further explore the unique Landau-level structure and quantum oscillation of the hybrid WSM. Based on our results, we propose that the hybrid WSM may be found in magnetically ordered noncentrosymmetric materials.

We start from the classification of the type-I and type-II Weyl nodes following Refs. [14] and [15]. Due to the linear band touching, the original pair of Weyl nodes with opposite chiralities has an emergent Lorentz invariance at low energies, and the gapless elementary excitation near the nodes are often called "Weyl fermions". The Lorentz invariance, however, is broken by the lattice regularization that necessarily connects the two Weyl nodes at high energy [20]. Significantly, this leads to the intactness of anomalous Hall effect but the breakdown of chiral magnetic effect. More seriously, the violation of Lorentz invariance in condensed-matter systems allows the tilting of Weyl nodes, as described in the following general

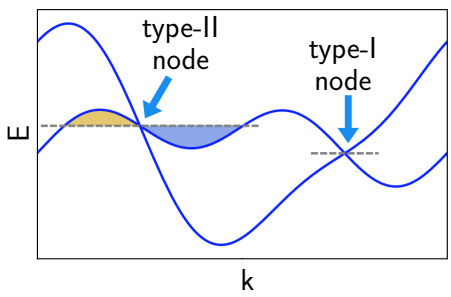

FIG. 1. A schematic band structure of a hybrid WSM with a pair of Weyl nodes. The left (right) node is a type-II (type-I) Weyl node. Generically, the energies of these two Weyl nodes cannot be identical when both time-reversal and inversion symmetries are absent.

*gchen_physics@fudan.edu.cn

$k \cdot p$ Hamiltonian near a Weyl node:

$$h_{\text{Weyl}}(\boldsymbol{k}) = \sum_{ij} k_i v_{ij} \sigma_j + \sum_i k_i u_i, \tag{1}$$

where $i,j = x,y,z$. Interestingly, the sign of $\bar{v} - 1$, with $\bar{v}_i = \sum_j v_{ij}^{-1} u_j$, defines the type of Weyl node:

$$\bar{v} < 1 \;\Rightarrow\; \text{type I}, \tag{2}$$

$$\bar{v} > 1 \;\Rightarrow\; \text{type II}. \tag{3}$$

For type-I nodes, the tilting is not too strong, and only energy anisotropy in momentum develops near the node. For type-II nodes, the tilting is sufficiently strong such that the Weyl node develops a structure [15], i.e., a "bouquet" of two spheres in mathematics, as depicted in Fig. 1. Physically, this implies that electron and hole Fermi pockets touch at the Weyl node. As shown in Ref. [15], an isolated "bouquet" enjoys the same first Chern number of the original Weyl node, while the electron or hole pocket is characterized by a zeroth Chern number, i.e., the difference in hole-band number across the Fermi sphere. In general, a Weyl node is characterized by its chirality and its type. The chirality cannot be changed by any local perturbation due to its topological protection by the unaltered Chern number. The type, however, can be modified by local disturbance through a topological transition in the zeroth Chern numbers, which twists the electron (hole) band down (up) near the Weyl node, as depicted in Fig. 1. In order to separately manipulate the types of the two Weyl nodes with opposite chiralities, any symmetry, e.g., inversion or antiunitary particle-hole symmetry, that relates the two nodes must then be broken. This is suggestive of the fundamental existence of a pair of hybrid Weyl nodes with opposite chiralities: one in type I and the other in type II.

We here propose a two-band tight-binding model of fermion hopping on a simple cubic lattice. At low energy this minimal model captures the essential physics of one pair of Weyl nodes with opposite chiralities. In real crystalline solids, it may represent a lattice regularization for a WSM or a Weyl superconductor; in cold atom systems, it may directly describe a Weyl superfluid or an artificial optical lattice with Weyl nodes. Nevertheless, such a Hamiltonian may be written as

$$\begin{aligned} H = \sum_j [& -t_x \boldsymbol{c}_j^\dagger \sigma_x \boldsymbol{c}_{j+\hat{x}} - t_y \boldsymbol{c}_j^\dagger \sigma_x \boldsymbol{c}_{j+\hat{y}} - t_z \boldsymbol{c}_j^\dagger \sigma_x \boldsymbol{c}_{j+\hat{z}} \\ & - i t_y' \boldsymbol{c}_j^\dagger \sigma_y \boldsymbol{c}_{j+\hat{y}} - i t_z' \boldsymbol{c}_j^\dagger \sigma_z \boldsymbol{c}_{j+\hat{z}} + \text{H.c.}] + m \boldsymbol{c}_j^\dagger \sigma_x \boldsymbol{c}_j. \end{aligned} \tag{4}$$

Here $\boldsymbol{c}^\dagger = (c_\uparrow^\dagger, c_\downarrow^\dagger)$ are the creation operators of fermions with spin $\uparrow$ and $\downarrow$, in which the Pauli matrices $\boldsymbol{\sigma}$ act on; $\boldsymbol{t}$ and $\boldsymbol{t}'$ are the hopping energies and m is the on-site energy, which are all spin dependent; $\hat{x},\hat{y},\hat{z}$ are the three first neighbor vectors on the cubic lattice. In momentum space, the Hamiltonian Eq. (4) reads

$$\begin{aligned} h(\boldsymbol{k}) = & (m - 2t_x \cos k_x - 2t_y \cos k_y - 2t_z \cos k_z)\sigma_x \\ & + 2t_y' \sin k_y \sigma_y + 2t_z' \sin k_z \sigma_z. \end{aligned} \tag{5}$$

One can easily demonstrate that there exists one pair of Weyl nodes at $\boldsymbol{q}_\pm = (\pm k_0, 0, 0)$ in the bulk Brillouin zone, and that the Fermi velocities are $\boldsymbol{v}_\pm = (\pm 2t_x \sin k_0, 2t_y', 2t_z')$ at the nodes, where $\cos k_0 = (m/2 - t_y - t_z)/t_x$. One can also check that in this model both time-reversal and inversion symmetries are broken, as

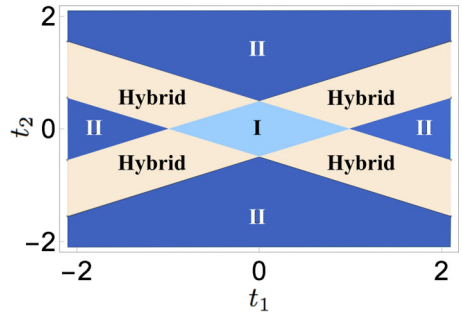

FIG. 2. The WSM diagram in t_1-t_2 plane with $\phi_1 = \pi, \phi_2 = \pi/2$. In the light (dark) blue region, type-I (type-II) WSM is realized. In the remaining part of the diagram, hybrid WSM is obtained. See the main text for the detailed discussion.

$$\mathcal{T} h(\boldsymbol{k}) \mathcal{T}^{-1} \neq h(-\boldsymbol{k}), \tag{6}$$

$$\mathcal{P} h(\boldsymbol{k}) \mathcal{P}^{-1} \neq h(-\boldsymbol{k}), \tag{7}$$

where $\mathcal{T} = \sigma_y K$, $\mathcal{P} = I_{2\times 2}$, K is the complex conjugation, and $I_{2\times 2}$ is an identity matrix. Such broken symmetries allow the presence of Weyl nodes, but their energies are not necessarily the same. However, there are emergent inversion-like and antiunitary particle-hole symmetries in the model, i.e., $\sigma_x h(\boldsymbol{k}) \sigma_x = h(-\boldsymbol{k})$ and $\sigma_z h(\boldsymbol{k}) \sigma_z = -h^*(-\boldsymbol{k})$. The former dictates the two nodes to appear at the same energy.

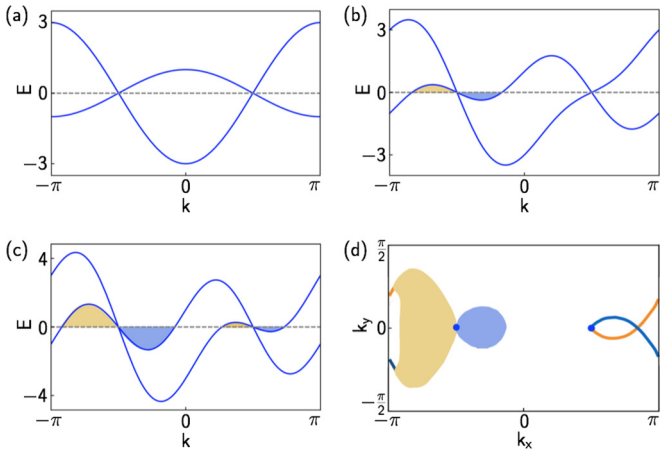

FIG. 3. The band structure along k_x direction and the surface states of different WSMs with representative parameters: (a) $t_1 = 0.5, t_2 = 0$, type-I WSM. (b) $t_1 = 0.5, t_2 = 0.5$, hybrid WSM. (c) $t_1 = 0.5, t_2 = 1$, type-II WSM. The hole pocket (in orange) and the electron pocket (in light blue) near the type-II node are indicated. (d) Surface Fermi arcs of a finite slab along the (001) direction for the hybrid WSM in (b). Two Weyl nodes (at the blue dots) are projected to $(\pm\pi/2, 0)$ in the surface Brillouin zone (k_x-k_y plane). The orange (blue) area is the projected hole (electron) pocket. The orange (blue) arc is localized on the top (bottom) surface and connects the hole pocket with the type-I node. The lattice constant is set to unity.

The inversion-like and the antiunitary particle-hole symmetries both dictate the identical type of the two Weyl nodes. Based on the classification criteria, both nodes are of type I, since $\bar{\boldsymbol{v}}_{\pm} = \boldsymbol{u} = 0$ in the model. In order to convert the type-I Weyl nodes into other types, we may introduce additional first and second neighbor hoppings into the Hamiltonian as follows:

$$H' = \sum_j [t_1 e^{-i\phi_1} \boldsymbol{c}_j^\dagger \boldsymbol{c}_{j+\hat{x}} + t_2 e^{-i\phi_2} \boldsymbol{c}_j^\dagger \boldsymbol{c}_{j+2\hat{x}} + \text{H.c.}], \quad (8)$$

which in momentum space can be expressed as

$$h'(\boldsymbol{k}) = 2t_1 \cos(\phi_1 - k_x) + 2t_2 \cos(\phi_2 - 2k_x). \quad (9)$$

Equation (8) describes the spin independent hopping processes along the x direction, and their phase dependence lifts the aforementioned inversionlike and antiunitary particle-hole symmetries, as long as not both of the two phases are integer multiples of π. Thus, $h'(\boldsymbol{k})$ generically leads to different energy modulations of the two original Weyl nodes. Intriguingly, the position and the chirality of each Weyl node remain intact, though their energies are different.

To examine the types of the deformed Weyl nodes under the action of Eq. (8), we expand the total Hamiltonian $H + H'$ near $\boldsymbol{q}_{\pm}$ and obtain

$$h_{\pm}(\boldsymbol{p}) = \mp 2t \sin k_0 p_x \sigma_x + 2t p_y \sigma_y + 2t p_z \sigma_z + 2[t_1 \sin(\phi_1 \mp k_0) + 2t_2 \sin(\phi_2 \mp 2k_0)] p_x, \quad (10)$$

where the subindex "$\pm$" refers to the two Weyl nodes at $\boldsymbol{q}_{\pm}$ and we have let $-t_x = t'_y = t'_z = t$. To capture the essential physics, we set $t = 1$, $t_y = t_z = 2$, $m = 8$ throughout the Rapid Communication. By tuning other parameters $(t_1, t_2, \phi_1, \phi_2)$ and using the criteria in Eqs. (2) and (3), we can realize all three WSMs (i) $v_{\pm} < 1$, (ii) $v_{\pm} > 1$, and (iii) $v_+ > 1$, $v_- < 1$, or vice versa, that correspond to type-I WSM, type-II WSM, and hybrid WSM, respectively. The WSM diagram is depicted in Fig. 2. In Figs. 3(a)–3(c), we further depict the band structures of some representative parameters for each case. Although we have chosen the parameters to make two Weyl nodes occur at the same energy for hybrid WSM, no symmetry protects such degeneracy in the general situation. Due to the mixed types of Weyl nodes in the hybrid WSM, one could actually have one single Weyl fermion in the excitation spectrum of the hybrid WSM [see Fig. 3(b)].

The bulk Fermi surface and the surface states of the hybrid WSM in Fig. 3(b) are depicted in Fig. 3(d). Rather than directly connecting two Weyl nodes in the type-I WSM, the arcs start from the type-I node and terminate when overlapping with the projected area of the hole pocket.

Landau level structure. One intriguing property of a WSM is its Landau-level structure near the Weyl nodes. With both type-I and type-II Weyl nodes in its spectrum, the hybrid WSM provides a unique opportunity to observe the Landau-level structures of two distinct nodes in one system. For a type-I Weyl node, a simple $k \cdot p$ theory gives Landau levels with specific level indices for any direction of the magnetic field. The zeroth Landau level is chiral and contributes to a nonzero chiral anomaly. By contrast, the Landau-level structure of a type-II Weyl node depends on the direction of the magnetic field [14,21,22]. For the magnetic field along the tilted direction of the type-II Weyl node, each Landau level is still characterized by one specific level index and the zeroth chiral Landau level (CLL) remains. For the field normal to the tilted direction, however, the Landau level no longer has a well-defined level index because different level indices are now mixed by the kinetic term. Despite the absence of the specific Landau level indices, the magnetic field cannot open any energy gap at the type-II node. The gapless nature at the type-II node is required to cancel the nonzero chiral anomaly at the type-I node.

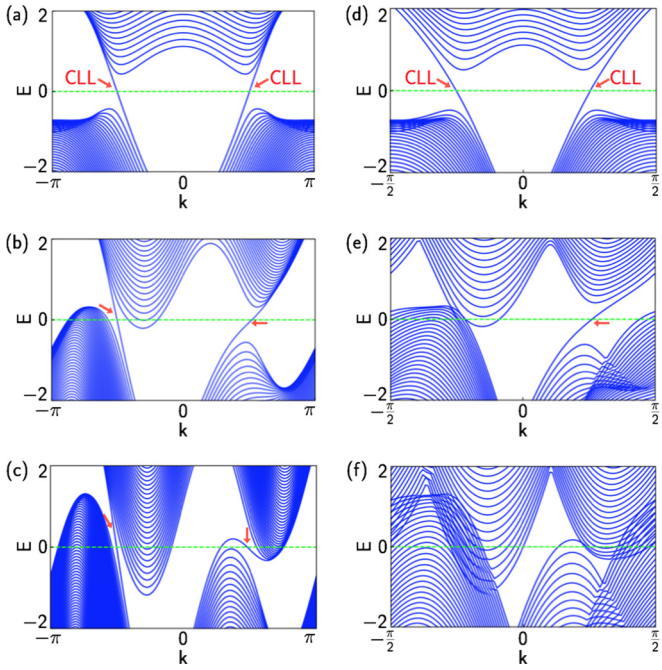

FIG. 4. The evolution of Landau level structures of different WSMs. The (red) arrows indicate the zeroth chiral modes near the (dashed) Fermi level. The left panels are the Landau levels along the momentum $(k,0,0)$ for field $\mathbf{B} = B[100]$, $t_1 = 0.5$ and (a) $t_2 = 0$ (type-I WSM); (b) $t_2 = 0.5$ (hybrid WSM); (c) $t_2 = 1$ (type-II WSM). The right panels are the Landau levels along the momentum $(k,k,0)$ for field $\mathbf{B} = B[110]$, $t_1 = 0.5$ and (d) $t_2 = 0$ (type-I WSM); (e) $t_2 = 0.5$ (hybrid WSM); (f) $t_2 = 1$ (type-II WSM). We have chosen the lattice Landau gauge and the magnetic field $B = 1/200\ \Phi_0$ where Φ_0 is the flux quantum.

With the lattice model, we explicitly explore the evolution of the Landau-level structure as the type of Weyl nodes and the WSMs are varied. When the magnetic field is along (100) direction, i.e., the tilted direction of the Weyl nodes, two CLLs at the two nodes of the type-I WSM remain recognizable even for the type-II and the hybrid WSMs (see the left panels in Fig. 4). By comparison, when the magnetic field is no longer parallel to the tilted direction of the Weyl nodes, e.g., along the (110) direction, the Landau-level structure behaves rather differently (see the right panels in Fig. 4). The CLL hybridizes with other levels when the corresponding Weyl node becomes type II. Dictated by the chiral anomaly cancellation, the type-II Weyl node remains gapless in the hybrid WSM. In type-II WSM, however, both two CLLs are not recognizable.

Quantum oscillation. Now we discuss the quantum oscillation of the hybrid WSM. Quantum oscillation directly probes the Fermi surface. For the type-I WSM with pointlike

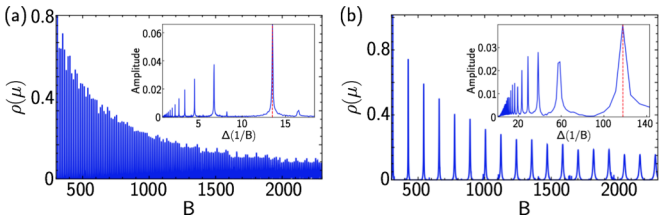

FIG. 5. The oscillation behavior of the density of states $\rho(\mu,k_x)$ for the hybrid WSM in Fig. 3(b). $\mathbf{B} = B(1,0,0)$. Fourier spectra in the insets indicate the oscillation periods $\Delta(B^{-1})$ (in the red line). Other peaks are higher harmonic components, $\frac{1}{2}\Delta(B^{-1}), \frac{1}{3}\Delta(B^{-1}), \ldots$. (a) The extremal cross section of the hole pocket occurs at $k_x = -2.4$ and has an area $0.296\pi^2$, and $\Delta(B^{-1}) = 13.5$. (b) The extremal cross section of the electron pocket occurs at $k_x = -1$ and has an area $0.034\pi^2$, and $\Delta(B^{-1}) = 117.8$. In the recursive Green's-function method [24], the real-space degrees of freedom along z direction is treated recursively. We set the system size $L_z = 10^5$ and choose an imaginary part $\delta = 10^{-4}$ for the level broadening.

Fermi surface, there is no oscillation from the bulk due to the vanishing density of states. It was, however, realized that the surface states of a finite slab could contribute to quantum oscillation and the period depends on the thickness of the slab [23]. For the hybrid WSM, there are electron and hole pockets at the type-II node. Therefore, the bulk quantum oscillation in a hybrid WSM directly detects the electron and hole pockets contacting at the type-II node.

Using the recursive Green's-function method [24], we numerically demonstrate the oscillatory behavior of the density of states $\rho(\mu,k_x)$. Here $\rho(\mu,k_x)$ is the density of states of the two-dimensional subsystem $h(\boldsymbol{k}) + h'(\boldsymbol{k})$ with a specified k_x component, and μ is Fermi energy chosen as the energy of the nodes. The results are presented in Fig. 5, for the magnetic field along (100) direction in the Landau gauge. The oscillation period of $\rho(\mu,k_x)$, $\Delta(B^{-1})$, is related to the cross-section area S of the Fermi surface at k_x with $S = 4\pi^2/\Delta(B^{-1})$. In Fig. 5, we have chosen two extremal cross sections of the electron and the hole pockets.

As we have tuned the Fermi energy at the nodes, only the electron and hole pockets at the type-II nodes contribute to the oscillation periods. Thus, two periods are found in Fig. 5. In the more general case, when the Fermi energy slightly deviates from the nodes, the electron (or hole) pocket at the type-I node would give another period in the quantum oscillation, and the total number of oscillation periods would be odd. As a comparison, for the conventional type-I WSM or type-II WSM where two Weyl nodes with opposite chiralities are related by certain symmetries, the density of states at two Weyl nodes would behave identically, and the number of oscillation periods should be even if the oscillation periods at each node can be separately resolved.

Discussion. Going beyond the concrete lattice model, we ask the necessary conditions to find the hybrid WSMs in physical systems. In the search of WSMs, one guiding principle is to look for systems that break either time-reversal or inversion symmetry [5,7]. This is because with both symmetries the Berry curvature vanishes at every point in the momentum space and cannot lead to any monopole singularity that was required for a WSM. To create monopole singularities of the Berry curvature, the necessary condition is to break either time-reversal or inversion symmetry. The recent discovery of type-I WSMs in the TaAs family and type-II WSMs in WTe_2 both belong to the inversion symmetry-breaking case [11,12,14]. In TaAs and WTe_2, the pair of Weyl nodes belong to the same type due to time-reversal symmetry. To search for hybrid WSM with mixed types of Weyl nodes, one should find systems that lack both inversion and time-reversal symmetries. We here propose that the magnetically ordered noncentrosymmetric materials are natural systems that host hybrid WSMs. Among the existing WSMs, TaAs and WTe_2 do not have inversion symmetry. To possibly convert them into hybrid WSMs, one could dope these materials with magnetic ions and create magnetic orders in them. Alternatively, one could introduce the inversion symmetry breaking in the WSMs with magnetic orders.

To summarize, we present a lattice model to realize three distinct WSMs. In addition to the WSMs that were previously known, we demonstrate the existence of a hybrid WSM with mixed types of Weyl nodes. The Landau-level structure and the quantum oscillation behaviors of the hybrid WSM are discussed. We discuss the physical conditions for possible realizations of hybrid WSMs and propose that they may be found in magnetically ordered noncentrosymmetric materials.

Acknowledgments. We thank Dr. Y. Qi for the positive comments. This work was supported by the 973 Program of MOST of China, Grant No. 2012CB821402, NNSF of China, Grants No. 11174298 and No. 11474061 (F.-Y.L., X.L., Y.Y.), NNSF of China, the 973 program of China, Grant No. 2013CB921700, and the "Strategic Priority Research Program (B)" of the Chinese Academy of Sciences, Grant No. XDB07020100 (X.D.), UT Dallas research enhancement funds (F.Z.), and the Start-up Fund of Fudan University and the National Thousand-Youth-Talent Program of People's Republic of China (F.-Y.L., G.C.).

F.-Y.L. and X.L. contributed equally.

[1] M. Z. Hasan and C. L. Kane, Rev. Mod. Phys. **82**, 3045 (2010).
[2] X.-L. Qi and S.-C. Zhang, Rev. Mod. Phys. **83**, 1057 (2011).
[3] G. Volovik, *The Universe in a Helium Droplet* (Oxford University Press, Oxford, 2003).
[4] S. Murakami, New J. Phys. **9**, 356 (2007).
[5] X. Wan, A. M. Turner, A. Vishwanath, and S. Y. Savrasov, Phys. Rev. B **83**, 205101 (2011).
[6] A. A. Burkov and L. Balents, Phys. Rev. Lett. **107**, 127205 (2011).
[7] A. M. Turner and A. Vishwanath, arXiv:1301.0330.
[8] G. Chen and M. Hermele, Phys. Rev. B **86**, 235129 (2012).
[9] S. A. Yang, H. Pan, and F. Zhang, Phys. Rev. Lett. **113**, 046401 (2014).

[10] D. Bulmash, P. Hosur, S.-C. Zhang, and X.-L. Qi, Phys. Rev. X **5**, 021018 (2015).

[11] S.-Y. Xu, I. Belopolski, N. Alidoust, M. Neupane, G. Bian, C. Zhang, R. Sankar, G. Chang, Z. Yuan, C.-C. Lee, S.-M. Huang, H. Zheng, J. Ma, D. S. Sanchez, B. Wang, A. Bansil, F. Chou, P. P. Shibayev, H. Lin, S. Jia, and M. Z. Hasan, Science **349**, 613 (2015).

[12] B. Q. Lv, H. M. Weng, B. B. Fu, X. P. Wang, H. Miao, J. Ma, P. Richard, X. C. Huang, L. X. Zhao, G. F. Chen, Z. Fang, X. Dai, T. Qian, and H. Ding, Phys. Rev. X **5**, 031013 (2015).

[13] L. Lu, Z. Wang, D. Ye, L. Ran, L. Fu, J. D. Joannopoulos, and M. Soljačić, Science **349**, 622 (2015).

[14] A. A. Soluyanov, D. Gresch, Z. Wang, Q. Wu, M. Troyer, X. Dai, and B. A. Bernevig, Nature (London) **527**, 495 (2015).

[15] Y. Xu, F. Zhang, and C. Zhang, Phys. Rev. Lett. **115**, 265304 (2015).

[16] F.-Y. Li, Y.-D. Li, Y. B. Kim, L. Balents, Y. Yu, and G. Chen, arXiv:1602.04288.

[17] A. A. Zyuzin and A. A. Burkov, Phys. Rev. B **86**, 115133 (2012).

[18] F.-Y. Li, Y.-D. Li, Y. Yu, and G. Chen, arXiv:1607.05618.

[19] T. M. McCormick, I. Kimchi, and N. Trivedi, arXiv:1604.03096.

[20] M. M. Vazifeh and M. Franz, Phys. Rev. Lett. **111**, 027201 (2013).

[21] T. E. O'Brien, M. Diez, and C. W. J. Beenakker, Phys. Rev. Lett. **116**, 236401 (2016).

[22] Z.-M. Yu, Y. Yao, and S. A. Yang, Phys. Rev. Lett. **117**, 077202 (2016).

[23] A. C. Potter, I. Kimchi, and A. Vishwanath, Nat. Commun. **5**, 5161 (2014).

[24] Y. Zhang, A. V. Maharaj, and S. Kivelson, Phys. Rev. B **91**, 085105 (2015).